Provided for non-commercial research and education use.
Not for reproduction, distribution or commercial use.

This article appeared in a journal published by Elsevier. The attached copy is furnished to the author for internal non-commercial research and education use, including for instruction at the authors institution and sharing with colleagues.

Other uses, including reproduction and distribution, or selling or licensing copies, or posting to personal, institutional or third party websites are prohibited.

In most cases authors are permitted to post their version of the article (e.g. in Word or Tex form) to their personal website or institutional repository. Authors requiring further information regarding Elsevier's archiving and manuscript policies are encouraged to visit:

http://www.elsevier.com/copyright

International Journal of Engineering Science 124 (2018) 104–114

Contents lists available at ScienceDirect

International Journal of Engineering Science

journal homepage: www.elsevier.com/locate/ijengsci

# Prismatic bifurcations of soft dielectric tubes

Eliana Bortot[1], Gal Shmuel*

*Faculty of Mechanical Engineering, Technion–Israel Institute of Technology, Haifa 32000, Israel*

ARTICLE INFO

*Article history:*
Received 14 July 2017
Revised 18 September 2017
Accepted 7 November 2017

ABSTRACT

Dielectric elastomer tubes are employed as actuators by radial electric stimulus. Their functionality is affected by electromechanical instabilities, whose study was mainly limited to the analysis of the free energy Hessian. In this paper, we identify a different class of instabilities—prismatic diffuse modes—by employing the linearized theory of superposed deformations on finitely strained deformable dielectrics. We develop the equations that determine the onset of such modes, and show through numerical examples that the tube may enter diffuse states before the Hessian criterion fails. Moreover, we find that loading paths that are stable according to the Hessian method, can bifurcate into diffuse modes.

© 2017 Elsevier Ltd. All rights reserved.

## 1. Introduction

The discovery that dielectric elastomers undergo reversible large deformations when subject to voltage (Pelrine et al., 2000; Pelrine, Kornbluh, Pei, & Joseph, 2000) has led to an extensive study of their functionality as actuators (Carpi & De Rossi, 2004; Carpi, De Rossi, Kornbluh, Pelrine, & Sommer-Larsen, 2008; O'Halloran, O'Malley, & McHugh, 2008). One of the fundamental configurations considered is a thin-walled tube, actuated by voltage between flexible electrodes coating its inner and outer surfaces (Carpi & De Rossi, 2004; Kornbluh, 2008; Pelrine, Kornbluh, & Joseph, 1998). The response of the actuator depends on geometrical and material nonlinearities, and therefore susceptible to electromechanical instabilities (De Tommasi, Puglisi, Saccomandi, & Zurlo, 2010; Lu, Cheng, Li, Wang, & Suo, 2016; Plante & Dubowsky, 2006; Siboni, Avazmohammadi, & Castañeda, 2014; Wang, Tahir, Zhang, & Zhao, 2011; Zhou, Hong, Zhao, Zhang, & Suo, 2008). Such instabilities can either result in unwanted electric breakdown (Plante & Dubowsky, 2006; Zurlo, Destrade, De Tommasi, & Puglisi, 2017), or harnessed for specific applications (Bortot & Shmuel, 2017; Keplinger, Li, Baumgartner, Suo, & Bauer, 2012; Shivapooja et al., 2013; Zhao & Wang, 2014).

The standard approach to predict the onset of instability in a deformable dielectric is to find when the Hessian of the free energy of the system is no longer positive definite (Leng, Liu, Liu, Yu, & Sun, 2009; Zhao & Suo, 2007). Recently, it has been recognized that this method is not sufficient to detect diffuse buckling modes. As discussed by Dorfmann and Ogden (2014) and Yang, Zhao, and Sharma (2017), the Hessian analysis of a dielectric elastomer film (thin plate) assumes that the surfaces remain plane, and hence cannot identify diffuse modes. To spot such bifurcations, the proper approach is to establish solutions in the form of diffuse modes to the equations of incremental deformations in finitely strained deformable dielectrics (Dorfmann & Ogden, 2010). In addition to the works of Dorfmann and Ogden (2014), Gei, Colonnelli, and Springhetti (2014), Yang et al. (2017) and Díaz-Calleja, Llovera-Segovia, and Quijano-López (2017) who analyzed plates, this approach was employed by Dorfmann and Ogden (2010) to study surface instabilities, and by Bertoldi and Gei (2011) to investigate instabilities in a laminate.

* Corresponding author.
*E-mail address:* meshmuel@tx.technion.ac.il (G. Shmuel).
[1] Now at Structural Engineering Department, University of California, San Diego, USA.

https://doi.org/10.1016/j.ijengsci.2017.11.002
0020-7225/© 2017 Elsevier Ltd. All rights reserved.

Reviewing the available literature shows that a rigorous analysis of diffuse mode instabilities in soft dielectric tubes—the objective of this work—has yet to be executed. Zhu, Stoyanov, Kofod, and Suo (2010) have used the Hessian method to analyze the tube when subject to radial voltage and axial force. The Hessian method tests only against perturbations that are similar to the primary loading path. Accordingly, the latter analysis examines only variations that maintain the circular shape of the tube. (Similarly, the Hessian of the film is evaluated against perturbations that maintain its rectangular shape.) Zhou, Jiang, and Khayat (2014) have considered mechanical buckling due to radial pressure by a rigid sleeve, using a simplified linear elasticity model. Lu, An, Li, Yuan, and Wang (2015) analyzed bulging instability following their experimental work (An, Wang, Cheng, Lu, & Wang, 2015), using a one-dimensional model. Su, Zhou, Chen, and Lü (2016) have properly employed the incremental theory to study buckling, however the underlying homogeneous deformation they considered is somewhat impractical, as the voltage therein is applied in the axial direction rather than the thin radial direction.

To proceed to our bifurcation analysis, we first summarize in Section 2 the theory of nonlinear electroelasticity, and its linearized version about a deformed configuration (deBotton, Tevet-Deree, & Socolsky, 2007; Dorfmann & Ogden, 2005; 2010; Liu, 2013; Suo, Zhao, & Greene, 2008). In Section 3 we recapitulate the large deformation and 'Hessian' instabilities of a dielectric elastomer tube due to radial voltage (Singh & Pipkin, 1966; Zhou et al., 2014; Zhu et al., 2010). Using the theory in Section 2, we formulate the equations governing incremental displacements relative to the configuration described in Section 3. Our formulation accounts for the electromechanical coupling, underlaying finite deformation and material nonlinearities. To solve the incremental equations, we postulate a solution in the form of prismatic diffuse modes, and employ a numerical scheme to obtain the bifurcation condition for its existence. This analysis is detailed in Section 4. We investigate in Section 5 how the critical voltage for bifurcation depends on the thickness of the tube and its mechanical constraints, using numerical results. We compare our instability results with the Hessian analysis. We find that a tube without axial constraints may bifurcate before the Hessian criterion fails. Moreover, we find that a tube whose axial length is fixed and its Hessian is always positive definite, can still enter diffuse modes. The paper is concluded with a recap of our main results in Section 6.

## 2. Theoretical framework

We consider an incompressible dielectric body occupying the volume $\Omega_0 \in \mathbb{R}^3$ and bounded by $\partial\Omega_0$ in a reference configuration. When subjected to electromechanical loads, the body deforms to its current configuration $\Omega$, bounded by $\partial\Omega$. The quasi-static deformation is represented by a smooth vector field $\boldsymbol{\chi}$, which maps material points $\mathbf{X}$ from the reference configuration to their current configuration $\mathbf{x}$, *i.e.*, $\mathbf{x} = \boldsymbol{\chi}(\mathbf{X})$. The deformation gradient $\frac{\partial \boldsymbol{\chi}}{\partial \mathbf{X}}$ is denoted by $\mathbf{F}$. The determinant of $\mathbf{F}$ is the volume ratio between deformed and referential volume elements, and Hence $\det \mathbf{F} = 1$, on account of incompressibility.

The equations of electrostatics in the deformed body are

$$\nabla \cdot \mathbf{d} = 0, \quad \nabla \times \mathbf{e} = \mathbf{0}, \tag{1}$$

where $\mathbf{e}$ and $\mathbf{d}$ are the electrical field and electric displacement field, respectively, and the differential operators are evaluated with respect to $\mathbf{x}$. The equation of electromechanical equilibrium is

$$\nabla \cdot \boldsymbol{\sigma} = \mathbf{0}, \tag{2}$$

where $\boldsymbol{\sigma}$—the *total* stress tensor—is symmetric to satisfy the balance of angular momentum.

The formulation is concluded with electromechanical jump conditions at the boundary, recalling that in the general case there are fields in the surrounding space to be accounted for (Bertoldi & Gei, 2011; Dorfmann & Ogden, 2005). Using superscript $\star$ to denote quantities outside the body, these conditions read

$$(\boldsymbol{\sigma} - \boldsymbol{\sigma}^\star)\mathbf{n} = \mathbf{t}_\mathrm{m}, \quad (\mathbf{e} - \mathbf{e}^\star) \times \mathbf{n} = \mathbf{0}, \quad (\mathbf{d} - \mathbf{d}^\star) \cdot \mathbf{n} = -\omega_\mathrm{e}, \tag{3}$$

where $\mathbf{t}_\mathrm{m}$ is a prescribed mechanical traction, $\omega_\mathrm{e}$ is a prescribed surface charge density, and $\mathbf{n}$ denotes outward unit normal to the surface. Assuming the domain outside the body is vacuum, we have that

$$\boldsymbol{\sigma}^\star = \epsilon_0 \left[ \mathbf{e}^\star \otimes \mathbf{e}^\star - \frac{1}{2}(\mathbf{e}^\star \cdot \mathbf{e}^\star)\mathbf{I} \right], \quad \mathbf{d}^\star = \epsilon_0 \mathbf{e}^\star, \tag{4}$$

where $\epsilon_0$ is the vacuum permittivity.

A Lagrangian formulation is based on the *pull backs*

$$\mathbf{P} = \boldsymbol{\sigma}\mathbf{F}^{-\mathrm{T}}, \quad \mathbf{E} = \mathbf{F}^\mathrm{T}\mathbf{e}, \quad \mathbf{D} = \mathbf{F}^{-1}\mathbf{d}, \tag{5}$$

which we refer to as the total first Piola–Kirchhoff stress, Lagrangian electric and electric displacement fields, respectively. In the reference configuration, these fields satisfy

$$\nabla_\mathbf{X} \cdot \mathbf{D} = 0, \quad \nabla_\mathbf{X} \times \mathbf{E} = \mathbf{0}, \quad \nabla_\mathbf{X} \cdot \mathbf{P} = \mathbf{0}, \tag{6}$$

with the conditions

$$(\mathbf{P} - \mathbf{P}^\star)\mathbf{N} = \mathbf{t}_\mathrm{M}, \quad (\mathbf{E} - \mathbf{E}^\star) \times \mathbf{N} = \mathbf{0}, \quad (\mathbf{D} - \mathbf{D}^\star) \cdot \mathbf{N} = -\omega_\mathrm{E}, \tag{7}$$

where $\mathbf{t}_\mathrm{M}$, $\omega_\mathrm{E}$ and $\mathbf{N}$ are the counterparts of $\mathbf{t}_\mathrm{m}$, $\omega_\mathrm{e}$ and $\mathbf{n}$ in the reference configuration (Bertoldi & Gei, 2011). Here and henceforth, differential operators with subscript $\mathbf{X}$ correspond to differentiation with respect to the reference coordinates.

We adopt the theory of Dorfmann and Ogden (2005), and formulate the constitutive laws of the material using an *augmented* energy density function $\Psi(\mathbf{F}, \mathbf{D})$, such that

$$\mathbf{P} = \frac{\partial \Psi}{\partial \mathbf{F}} - p_0 \mathbf{F}^{-\mathrm{T}}, \qquad \mathbf{E} = \frac{\partial \Psi}{\partial \mathbf{D}}. \tag{8}$$

Here, the *Lagrange multiplier* $p_0$ accounts for the arbitrary stress ensuing from incompressibility.

Bucking instabilities are identified by investigating the existence of incremental deformations superposed on the deformed configurations. To this end, we revisit the incremental formulation developed in Dorfmann and Ogden (2010). Accordingly, we consider the increments $\dot{\boldsymbol{\chi}}(\mathbf{X})$ and $\dot{\mathbf{D}}(\mathbf{X})$ to a configuration close to $\Omega$, say $\Omega'$, conjugated with the increments $\dot{\mathbf{E}}$ and $\dot{\mathbf{P}}$. The theory of Dorfmann and Ogden (2010) develops the incremental equations derived from Eqs. (6) and (7), and the incremental constitutive relations derived from Eq. (8). We refer the readers to Dorfmann and Ogden (2010) for complete details, and for brevity provide only the resultant equations. Accordingly, the incremental equations are compactly expressed in terms of the *push forwards*

$$\boldsymbol{\Sigma} = \dot{\mathbf{P}}\mathbf{F}^{\mathrm{T}}, \quad \check{\mathbf{e}} = \mathbf{F}^{-\mathrm{T}}\dot{\mathbf{E}}, \quad \check{\mathbf{d}} = \mathbf{F}\dot{\mathbf{D}}, \tag{9}$$

namely,

$$\nabla \cdot \check{\mathbf{d}} = 0, \quad \nabla \times \check{\mathbf{e}} = \mathbf{0}, \quad \nabla \cdot \boldsymbol{\Sigma} = \mathbf{0}. \tag{10}$$

In case there are no external electric fields and the prescribed mechanical load is independent of the deformation, the incremental jump conditions across the deformed boundary are

$$\begin{aligned} \boldsymbol{\Sigma}\mathbf{n} &= \mathbf{0}, \\ \check{\mathbf{e}} \times \mathbf{n} &= \mathbf{0}, \\ \check{\mathbf{d}} \cdot \mathbf{n} &= -\check{\omega}_e, \end{aligned} \tag{11}$$

where $\check{\omega}_e$ is the increment in $\omega_E$ per deformed area element. Finally, upon linearization in the increments, the linearized constitutive laws are

$$\boldsymbol{\Sigma} = \mathscr{C}\mathbf{h} + p_0\mathbf{h} - \dot{p}_0\mathbf{I} + \mathscr{B}\check{\mathbf{d}}, \tag{12}$$

$$\check{\mathbf{e}} = \mathscr{B}^{\mathrm{T}}\mathbf{h} + \mathscr{A}\check{\mathbf{d}}, \tag{13}$$

where $\mathbf{h} = \nabla\dot{\mathbf{x}}$, $\dot{\mathbf{x}}(\mathbf{x}) \equiv \dot{\boldsymbol{\chi}}(\mathbf{X})$ are subjected to the incompressibility constraint

$$\nabla \cdot \dot{\mathbf{x}} = \mathrm{tr}\mathbf{h} = 0; \tag{14}$$

the action $\mathscr{B}^{\mathrm{T}}\mathbf{h}$ is defined by $\left(\mathscr{B}^{\mathrm{T}}\mathbf{h}\right)_k = \mathscr{B}_{ijk}\, h_{ij}$, and the *instantaneous* tensors $\mathscr{A}$, $\mathscr{B}$ and $\mathscr{C}$ are defined by

$$\mathscr{A}_{ij} = JF^{-1}_{\alpha i}\frac{\partial^2\Psi}{\partial D_\alpha \partial D_\beta}F^{-1}_{\beta j}, \quad \mathscr{B}_{ijk} = F_{j\alpha}\frac{\partial^2\Psi}{\partial F_{i\alpha}\partial D_\beta}F^{-1}_{\beta k}, \quad \mathscr{C}_{ijkl} = J^{-1}F_{j\alpha}\frac{\partial^2\Psi}{\partial F_{i\alpha}\partial F_{k\beta}}F_{l\beta}. \tag{15}$$

These tensors are the electroelastic moduli in the linearized constitutive relations. For further details, see Section 3.1. in Dorfmann and Ogden (2010).

## 3. Voltage-induced deformation of a soft dielectric tube

The quasi-static deformation of a soft tube by a radial electric field has been addressed in several works (Bortot & Shmuel, 2017; Cohen, 2017; Melnikov & Ogden, 2016; Shmuel & deBotton, 2013; Singh & Pipkin, 1966; Wu, Su, Chen, & Zhang, 2017; Zhou et al., 2014; Zhu et al., 2010). For compactness, we revisit only the geometry, boundary conditions and resultant deformation, and refer to above the Refs. for the complete solution.

An infinitely long dielectric tube is coated with compliant electrodes at its inner radius, $R_i$, and outer radius, $R_o$ (Fig. 1a). A quasi-static deformation of the tube is obtained by the application of a voltage $\Delta V$ to the electrodes (Fig. 1b). Assuming incompressibility, the deformation is

$$r = \sqrt{AR^2 + B}, \ \theta = \Theta, \ z = \frac{Z}{A}, \tag{16}$$

where $(R, \Theta, Z)$ and $(r, \theta, z)$ are the referential and the current cylindrical coordinates, respectively. The deformation gradient matrix is diagonal in the corresponding bases, with the principal stretches

$$\lambda_r = \frac{AR}{\sqrt{AR^2 + B}}, \ \lambda_\theta = \frac{\sqrt{AR^2 + B}}{R}, \ \lambda_z = \frac{1}{A}. \tag{17}$$

The unknowns $A$ and $B$ are determined once the constitutive behavior of the tube is specified, by solving the governing equations and boundary conditions. Thereby, the stretch-voltage relation is obtained. The outstanding issue is: *at which voltage the deformation bifurcates from its primary path?* The common approach is to find when the Hessian of the system

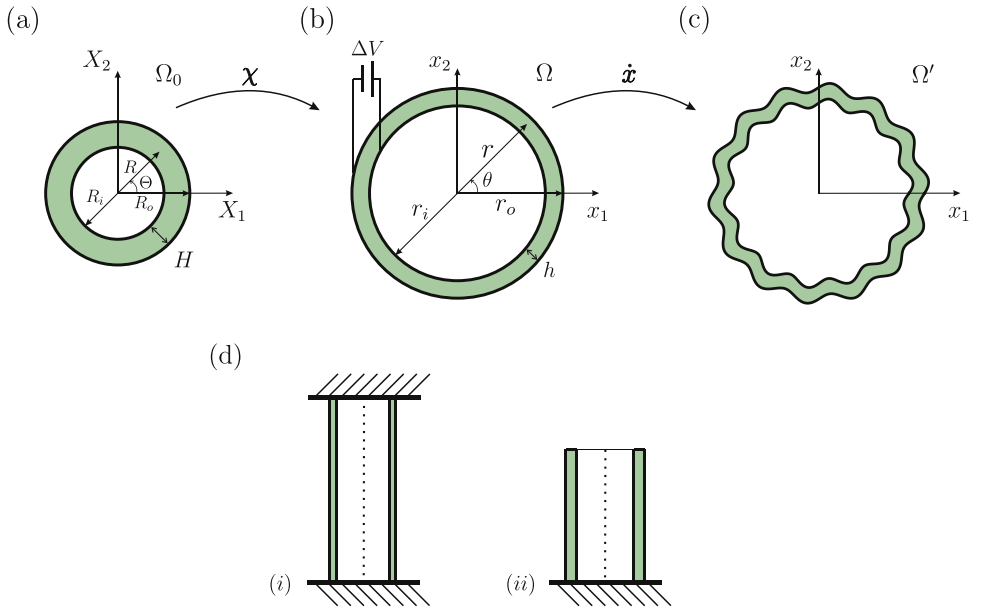


**Fig. 1.** Dielectric elastomer tube in (a) the reference configuration, and (b) the deformed configuration, when subject to voltage. (c) Diffuse modes superposed on the deformed deformation. (d) *i*. Axially clamped and *ii*. axially free tubes.

total energy is no longer positive definite (Díaz-Calleja, Riande, & Sanchis, 2008; Zhao & Suo, 2007). As mentioned, the latter is restricted only to perturbations that are similar to the primary loading path. Thus, the Hessian method identifies only homogeneous configurations of a film, and only configurations that maintain the circular shape of the tube. In the sequel, we identify another type of instabilities, namely, prismatic diffuse modes (Fig. 1c), where the tube remains prismatic while the cross-section looses its circular shape (Haughton & Ogden, 1979a). Importantly, we show that the tube may enter the latter modes of bifurcation *before* the Hessian criterion fails. For completeness, we revisit the conclusions drawn using the Hessian method, specialized to the cases when tube is (*i*) mechanically pre-stretched and clamped in the axial direction, and when it is (*ii*) free to deform in the axial direction (Fig. 1d).

The total energy of the system comprises the tube free energy and the potential energy of the voltage source. Thus, the total energy of a tube with initial length $L$ is

$$\Pi = \int_0^L \int_0^{2\pi} \int_{R_i}^{R_o} \Psi(\mathbf{F}, \mathbf{D}) R \mathrm{d}R \mathrm{d}\Theta \mathrm{d}Z - Q\Delta V, \tag{18}$$

where $Q$ is the total charge. Solutions that render $\Pi$ stationary are presented in Fig. 2a, in terms of the normalized voltage $\Delta\hat{V} = \frac{\Delta V}{H}\sqrt{\frac{\epsilon}{\mu}}$ and the outer circumferential stretch $\lambda_o = \lambda_\theta(R_o)$, for an axially free tube. The red curve corresponds to a Gentian tube, whose augmented energy is given by

$$\Psi(\mathbf{F}, \mathbf{D}) = -\frac{\mu J_m}{2} \ln\left[1 - \frac{\mathrm{tr}(\mathbf{F}^{\mathrm{T}}\mathbf{F}) - 3}{J_m}\right] + \frac{1}{2\epsilon}\mathbf{D} \cdot \mathbf{F}^{\mathrm{T}}\mathbf{F}\mathbf{D}, \tag{19}$$

where $\mu$ is the shear modulus, $\epsilon$ is the dielectric constant, and $J_m$ models the elastomeric strain stiffening. In the example, the material parameters used are $\mu = 350\,\mathrm{kPa}$, $J_m = 10$, and $\epsilon = 3\epsilon_0$, and the geometric parameters are $R_i = 10\,\mathrm{mm}$ and $R_0 = 12.5\,\mathrm{mm}$. Beyond the voltage $\Delta\hat{V} \simeq 0.68$ (point $C'$), there are multiple solutions that maintain the circular shape of the tube. Zhu et al. (2010) carried out an analysis based on the Hessian method, and showed that the solutions between $C'$ and $A$ are stable, while those between $A$ and $C$ are not. Therefore, the tube will not bifurcate from the primary path to the secondary path. Indeed, the total energy along the primary path is lower than the energy along the secondary path, as shown in Fig. 2c, which depicts the normalized total energy $\hat{\Pi} = \frac{\Pi}{\mu\pi L(R_o^2 - R_i^2)}$ versus $\Delta\hat{V}$. At the peak (point $A$), a *snap-through* instability is identified using the Hessian method (Keplinger et al., 2012; Li et al., 2013; Zhao & Suo, 2010). At this point, the tube bifurcates or *snaps* to state $A'$ (see also Fig. 7 in Zhu et al., 2010). In the sequel, we will show that the tube may still undergo buckling instabilities along the path $C' - A$, even though the path is stable according to the Hessian criterion. Corresponding plots for an axially fixed tube at $\tilde{\lambda}_z = 1$ (clamped without pre-stretch), and at the pre-stretches $\tilde{\lambda}_z = 1.5$ and 2 are shown in panels of Fig. 2b and d. As the Hessian criterion correlates with a local maximum in the voltage-stretch plane (see, *e.g.*, Fig. 3 in Zhu et al., 2010), the monotonicity of the curve which corresponds to the fixed tube indicates that the tube is stable according to the Hessian method (see also Fig. 4 in Zhou et al., 2014). In the sequel, we will show that the fixed tube can still experience buckling instabilities. For completeness, we also illustrate the response of a neo-Hookean

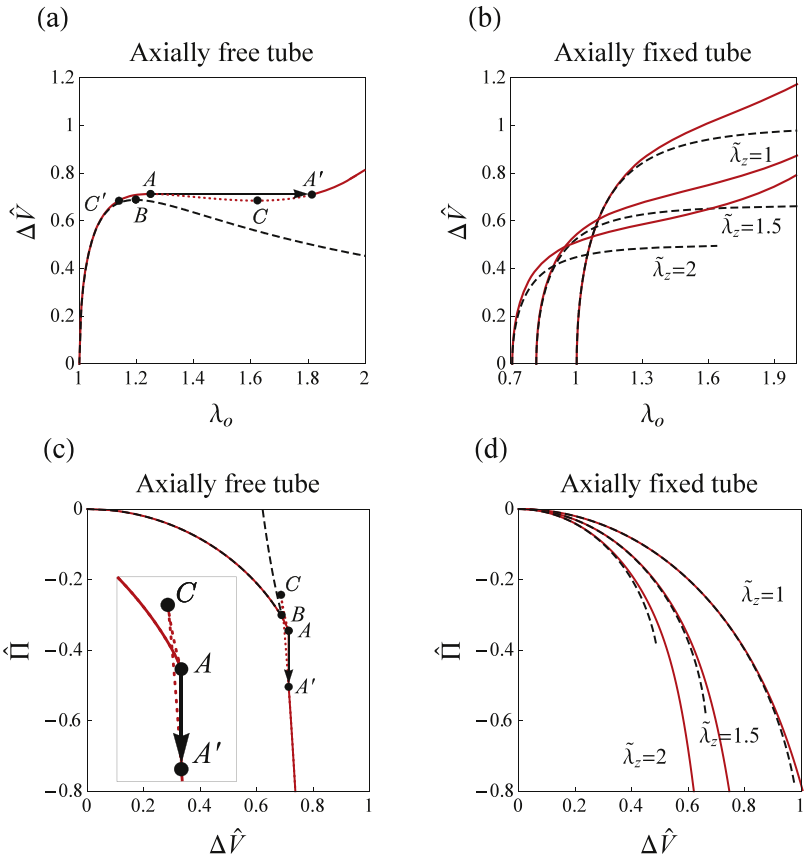


**Fig. 2.** (a,b) Normalized voltage $\Delta\hat{V}$ as function of the outer circumferential stretch $\lambda_o$. (c,d) Normalized total energy $\hat{\Pi}$ as function of the normalized voltage. Panels (a,c) correspond to an axially free tube, and Panels (b,d) correspond to a tubes clamped at the axial stretch ratios $\tilde{\lambda}_z = 1, 1.5$ and 2. Continuous and dashed lines denote the Gentian and the neo-Hookean tubes, respectively. Points *A* and *B* indicate the onset of snap-through and pull-in instabilities, respectively.

tube (black dashed curves in Fig. 2), whose constitutive model is a particular case of the Gentian energy in the limit $J_m \to \infty$. Since this model does not capture the elastomeric stiffening, a neo-Hookean tube cannot mechanically equilibrate Coulomb forces beyond the peak (point *B*), and, at this point, the Hessian method identifies the so-called *pull-in* instability (see also Fig. 3 in Zhu et al., 2010). The reader is referred to Plante and Dubowsky (2006) for a detailed discussion on the pull-in instability mode.

## 4. Prismatic bifurcations of actuated soft dielectric tubes

To identify prismatic bifurcations of the actuated tube, we examine circumferential diffuse modes utilizing the incremental equations in Section 2, specialized to the configuration presented in Section 3. First, we calculate in polar coordinates the instantaneous tensors $\mathscr{A}$, $\mathscr{B}$ and $\mathscr{C}$. When the Gent model (19) and the deformation gradient (17) are considered, the non-zero components of these tensors are (see also Shmuel, 2015; Shmuel & deBotton, 2013)

$$\mathscr{A}_{rr} = \mathscr{A}_{\theta\theta} = \mathscr{A}_{zz} = \frac{1}{\epsilon},$$

$$\mathscr{B}_{r\theta\theta} = \mathscr{B}_{rzz} = \mathscr{B}_{\theta r\theta} = \mathscr{B}_{zrz} = 2\mathscr{B}_{rrr} = e_r = \frac{d_r}{\epsilon},$$

$$\mathscr{C}_{rrrr} = \mu\frac{J_m}{\alpha}\lambda_r^2\left(1+\frac{2}{\alpha}\lambda_r^2\right) + \frac{1}{\epsilon}d_r^2,$$

$$\mathscr{C}_{\theta r\theta r} = \mathscr{C}_{zrzr} = \mu\frac{J_m}{\alpha}\lambda_r^2 + \frac{1}{\epsilon}d_r^2,$$

$$\mathscr{C}_{\theta\theta\theta\theta} = \mu\frac{J_m}{\alpha}\lambda_\theta^2\left(1+\frac{2}{\alpha}\lambda_\theta^2\right),$$

$$\mathscr{C}_{r\theta r\theta} = \mathscr{C}_{z\theta z\theta} = \mu\frac{J_m}{\alpha}\lambda_\theta^2,$$

$$\mathscr{C}_{zzzz} = \mu\frac{J_m}{\alpha}\lambda_z^2\left(1+\frac{2}{\alpha}\lambda_z^2\right),$$
$$\mathscr{C}_{\theta z\theta z} = \mathscr{C}_{rzrz} = \mu\frac{J_m}{\alpha}\lambda_z^2, \tag{20}$$

where $\alpha = J_m - (\lambda_r^2+\lambda_\theta^2+\lambda_z^2-3)$. In the neo-Hookean limit, as $J_m\to\infty$ the ratio $\frac{J_m}{\alpha}$ equals 1.

Restricting attention to prismatic bifurcations (Haughton & Ogden, 1979b), we consider an incremental displacement field independent of the $z$ coordinate, namely

$$\dot{\mathbf{x}}(r,\theta) = u(r,\theta)\hat{\mathbf{r}} + v(r,\theta)\hat{\boldsymbol{\theta}} + w(r,\theta)\hat{\mathbf{z}}. \tag{21}$$

We note that the incremental governing equation in the $z$ direction decouples from the other equations and reduces to an equation for $w$ alone. Therefore, we can set $w=0$ and address only the in-plane problem without loss of generality. Thus, the resultant in-plane displacement gradient matrix is

$$\mathsf{h} = \begin{bmatrix} u_{,r} & (u_{,\theta}-v)/r \\ v_{,r} & (u-v_{,\theta})/r \end{bmatrix}. \tag{22}$$

The incompressibility constraint (14) then takes the form

$$u_{,r} + \frac{1}{r}(u+v_{,\theta}) = 0. \tag{23}$$

The incremental equations of equilibrium along directions $r$ and $\theta$ are

$$\boldsymbol{\sigma}_{rr,r} + \frac{1}{r}\boldsymbol{\sigma}_{r\theta,\theta} + \frac{1}{r}(\boldsymbol{\sigma}_{rr}-\boldsymbol{\sigma}_{\theta\theta}) = 0, \tag{24a}$$

$$\boldsymbol{\sigma}_{\theta r,r} + \frac{1}{r}\boldsymbol{\sigma}_{\theta\theta,\theta} + \frac{1}{r}(\boldsymbol{\sigma}_{\theta r}+\boldsymbol{\sigma}_{r\theta}) = 0, \tag{24b}$$

respectively, where

$$\begin{aligned}
\boldsymbol{\sigma}_{rr} &= (\mathscr{C}_{rrrr}+p_0)h_{rr} - \dot{p}_0 + \mathscr{B}_{rrr}\check{d}_r,\\
\boldsymbol{\sigma}_{r\theta} &= \mathscr{C}_{r\theta r\theta}h_{r\theta} + p_0 h_{\theta r} + \mathscr{B}_{r\theta\theta}\check{d}_\theta,\\
\boldsymbol{\sigma}_{\theta\theta} &= (\mathscr{C}_{\theta\theta\theta\theta}+p_0)h_{\theta\theta} - \dot{p}_0,\\
\boldsymbol{\sigma}_{\theta r} &= \mathscr{C}_{\theta r\theta r}h_{\theta} + p_0 h_{r\theta} + \mathscr{B}_{\theta r\theta}\check{d}_\theta.
\end{aligned} \tag{25}$$

Incremental electric equations are addressed next, recalling that the voltage applied to the electrodes is fixed and $\mathbf{e}^\star = \dot{\mathbf{e}}^\star = \mathbf{0}$. The second of Eq. (10) is automatically satisfied by setting the incremental electric field $\check{\mathbf{e}}$ as the gradient of a scalar potential field $\varphi$, namely $\check{\mathbf{e}} = -\nabla\varphi$. The first of Eq. (10) in polar coordinates reads

$$\check{d}_{r,r} + \frac{\check{d}_r}{r} + \frac{1}{r}\check{d}_{\theta,\theta} = 0, \tag{26}$$

where

$$\begin{aligned}
\check{d}_r &= -\epsilon\varphi_{,r} - 2d_r h_{rr},\\
\check{d}_\theta &= -\epsilon\frac{1}{r}\varphi_{,\theta} - d_r h_{r\theta} - d_r h_{\theta r}.
\end{aligned} \tag{27}$$

We seek solutions in the form of the diffuse modes

$$\begin{aligned}
u &= h(r)\mathrm{e}^{\mathrm{i}k\theta},\\
v &= g(r)\mathrm{e}^{\mathrm{i}k\theta},\\
\varphi &= f(r)\mathrm{e}^{\mathrm{i}k\theta},\\
\dot{p}_0 &= q(r)\mathrm{e}^{\mathrm{i}k\theta}.
\end{aligned} \tag{28}$$

By substituting Eq. (28) into the incompressibility constraint (14), we obtain the relation between the functions $g(r)$ and $h(r)$, namely

$$g(r) = \frac{\mathrm{i}h(r) + \mathrm{i}rh'(r)}{k}. \tag{29}$$

Utilizing Eq. (29), we eliminate $g(r)$ from the remaining equations. By means of Eq. (24b), we express $q(r)$ in terms of $h(r)$, $f(r)$ and their derivatives. The derivative of the latter relation provides an expression for $q'(r)$, that we substitute into Eq. (24a). The resultant equation with Eq. (26) are coupled ordinary differential equations for $f$ and $h$. These equations are

cast in dimensionless form by normalizing with respect $R_i$, $\mu$ and $\epsilon$. The normalized equations are reformulated in terms of an equivalent set of six coupled linear differential equations of order 1 in the form

$$\frac{\mathrm{d}y_i}{\mathrm{d}r} = A_i(\mathbf{y}, r) \qquad i = 1, ..., 6, \tag{30}$$

where

$$\mathbf{y}(r) = \left\{ f,\ f',\ h,\ h',\ h'',\ h''' \right\}. \tag{31}$$

Eq. (30) is subjected to the boundary conditions (11) at the internal radius $r = r_i$ and external radius $r = r_o$ , namely,

$$\begin{array}{ll} \boldsymbol{\Sigma}_{rr}(r_i) = 0, & \boldsymbol{\Sigma}_{rr}(r_o) = 0, \\ \boldsymbol{\Sigma}_{r\theta}(r_i) = 0, & \boldsymbol{\Sigma}_{r\theta}(r_o) = 0, \\ \varphi(r_i) = 0, & \varphi(r_o) = 0. \end{array} \tag{32}$$

Note that the conditions on $\varphi$ result from applying a prescribed fixed voltage to the electrodes. Also note that the resultant incremental surface charge density can be found from the last of Eq. (11). Using a fourth-order Runge–Kutta method, Eq. (30) is integrated numerically, subject to the conditions

$$y_j^{(m)}(r_i) = \delta_{jm} \qquad j = 1, ..., 6, \tag{33}$$

where $\delta_{jm}$ is the Kronecker delta function. Thus, the six generated solutions $\mathbf{y}^{(m)}$ constitute a basis for the general solution of Eq. (30)

$$\mathbf{y} = \sum_{m=1}^{6} c_m \mathbf{y}^{(m)}, \tag{34}$$

where $c_m$ are six constants. The boundary conditions are written in terms of these constants, upon substitution of Eq. (34) into Eq. (32). Bifurcation occurs if there exists a non-trivial set $\{c_m\}$ such that the boundary conditions (32) are satisfied at $r_i$ and $r_o$. The condition for the existence of this set is derived setting the determinant of the coefficient matrix of $\{c_m\}$ to zero. This numerical technique was first used for purely elastic bifurcation problems (Ertepinar, 1978; Haughton & Ogden, 1979b; Ogden, Steigmann, & Haughton, 1997), and later extended to electroelastic wave propagation problems (Shmuel, 2015; Shmuel & deBotton, 2013).

## 5. Results

Using numerical solutions obtained through our scheme, we study how prismatic bifurcations are triggered by the applied voltage for different values of the tube thickness and different mechanical constraints. To this end, we consider the exemplary tube in Section 3, and examine different geometries by varying the ratio $H/\overline{R}$, where $H = R_o - R_i$ and $\overline{R} = (R_i + R_o)/2$.

We begin with an analysis of a tube free of axial constraints. Fig. 3a shows the critical voltage for diffuse instability versus the tube relative thickness $H/\overline{R}$. Fig. 3b shows the corresponding outer circumferential stretch versus $H/\overline{R}$. Herein and henceforth, the blue, orange, green, red and purple curves correspond to modes $k = 2, .., 6$, respectively. For comparison, the

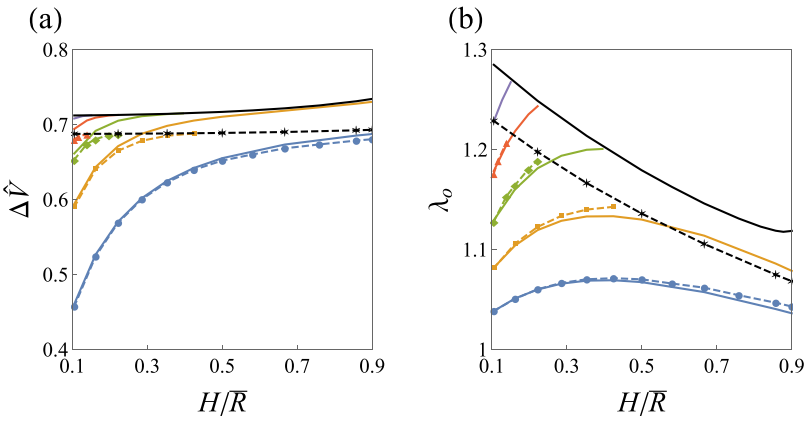


**Fig. 3.** *Axially free tube.* (a) Critical voltage $\Delta\hat{V}$ and (b) corresponding outer circumferential stretch $\lambda_o$ at which diffuse instability occurs, as functions of the thickness $H/\overline{R}$ , when $J_m = 10$ (continuous curves) and when the tube is neo-Hookean (dashed curves with marks). Blue, orange, green, red and purple curves correspond to modes $k = 2 - 6$, respectively. Continuous black curves and dashed black curves with marks correspond to instabilities identified by the Hessian method in the Gentian and neo-Hookean tubes, respectively. (For interpretation of the references to colour in this figure legend, the reader is referred to the web version of this article).

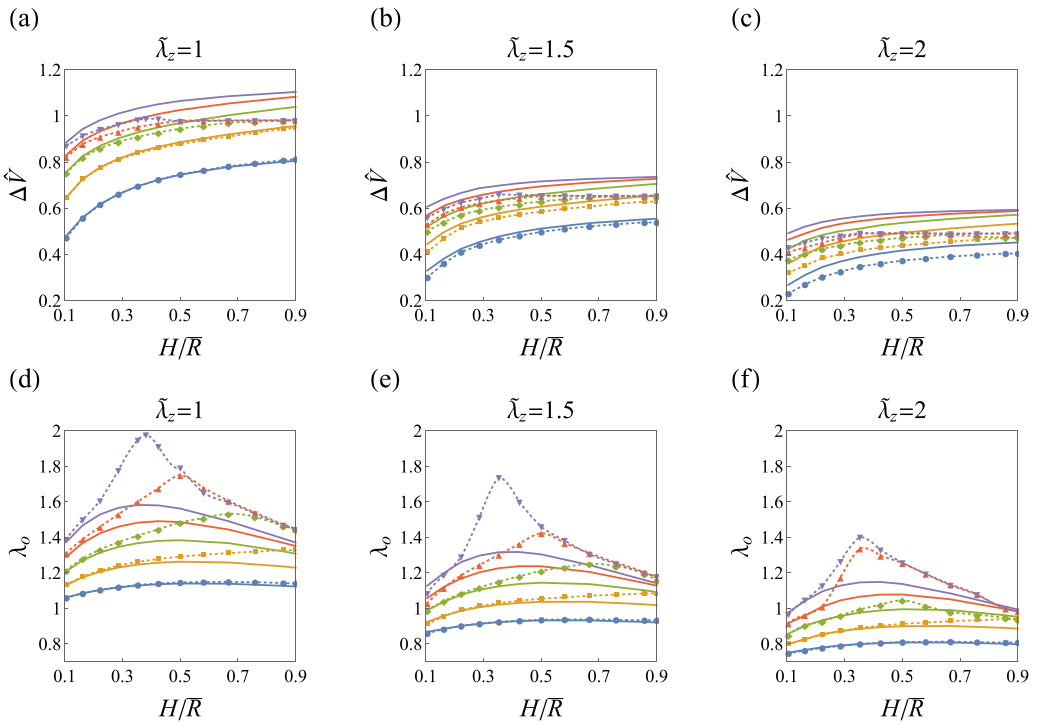


**Fig. 4.** *Axially fixed tube.* (a-c) Critical voltage $\Delta\hat{V}$ and (d-f) corresponding outer circumferential stretch $\lambda_o$ at which diffuse instability occurs, as functions of the thickness $H/\overline{R}$, when the tube is (a, d) clamped without pre-stretch $\left(\tilde{\lambda}_z = 1\right)$, and when clamped after pre-stretches of (b, e) $\tilde{\lambda}_z = 1.5$ and (c, f) $\tilde{\lambda}_z = 2$. Continuous curves correspond to $J_m = 10$, and dashed curves with marks correspond a neo-Hookean tube. Blue, orange, green, red and purple curves correspond to modes $k = 2-6$, respectively. (For interpretation of the references to colour in this figure legend, the reader is referred to the web version of this article).

black curves correspond to instabilities identified by the Hessian method. The continuous curves and the dashed curves with marks correspond to the Gentian and neo-Hookean tubes, respectively. We recall that the neo-Hookean model corresponds to the limit $J_m \to \infty$. Accordingly, results for tubes with $10 < J_m < \infty$ produce curves that vary continuously from the continuous curves to the dashed curves. These intermediate cases are not shown, for brevity. The most significant observation is that a lower voltage is required to trigger diffuse mode instabilities, than to trigger pull-in or snap-through instabilities. As expected, the required voltage increases monotonically with the thickness of the tube. The number of possible modes also depends on the thickness—it decreases when $H/\overline{R}$ increases. This number also depends on the elastomeric stiffening of the tube—the Gent model, which captures this stiffening, admits more diffuse modes. We also observe that higher diffuse modes require higher voltage to be triggered than lower modes.

We address next mechanically pre-stretched and clamped tube. We recall that under this axial constraint, the tube is stable according to the Hessian criterion; our analysis shows that the tube may still experience diffuse mode instabilities. To this end, in Fig. 4a–c we show the critical voltage for diffuse instability versus $H/\overline{R}$. Panels 4d–f show the corresponding outer circumferential stretch versus $H/\overline{R}$. The left, center and right panels correspond to an axial stretch of $\tilde{\lambda}_z = 1, 1.5$ and 2, respectively. Here again, continuous and dashed curves correspond to Gentian and neo-Hookean tubes, respectively. Again, results for tubes with $10 < J_m < \infty$ provide curves that transition from the continuous curves to the dashed curves.

Two observations that were made for the axially free tube are repeated for the clamped tube. (i) Thin tubes require less voltage to buckle than thick tubes. Note that beyond a certain thickness, however, the required voltage to trigger modes $4-6$ in the neo-Hookean tube slightly decreases. At that critical thickness we also observe a peak in the circumferential stretch. (ii) Higher voltage is required to trigger higher diffuse modes. In contrast with the free tube, here the number of modes does not depend on the thickness. Note that beyond a certain thickness, it appears that modes $4-6$ of the neo-Hookean tube coincide. A comparison of panels 4a–c reveals that pre-stretch reduces the critical voltage for diffuse instability modes. Thus, pre-stretch destabilizes the tube by promoting these modes, contrarily to its suppressing effect on the pull-in/snap-through modes (Jiang, Betts, Kennedy, & Jerrams, 2016; Li et al., 2011).

Finally, for illustration purposes, we show the tube configuration at the onset of circumferential buckling for the different axial settings examined. Specifically, Fig. 5 shows the mapping of the median surface, $r\left(\overline{R}\right)$, of a Gentian tube with $H/\overline{R} = 2/9$; panel 5a corresponds to the axially free tube, where panels 5b–d correspond to a tube clamped at $\tilde{\lambda}_z = 1, 1.5$ and 2, respectively. Note that since in our analysis we solve a homogeneous system of equations for the coefficients, the magnitude

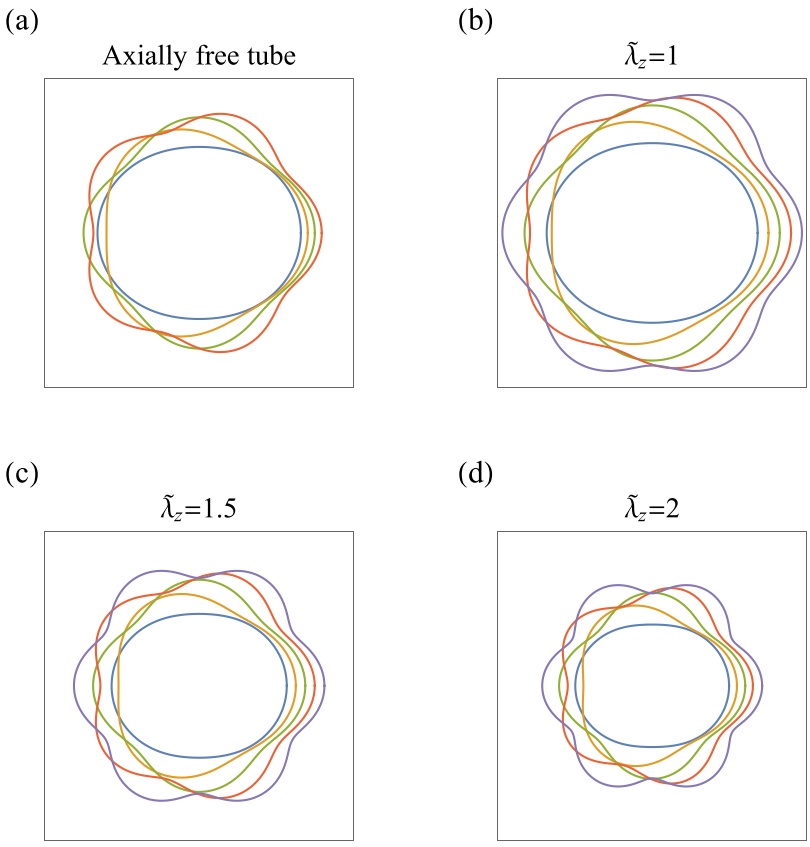


**Fig. 5.** Mapping of the median surface, $r(\overline{R})$, of a Gentian tube with $H/\overline{R} = 2/9$. Panel (a) corresponds to an axially free tube, and panels (b-d) correspond to a tube clamped at $\tilde{\lambda}_z = 1, 1.5$ and 2, respectively. The amplitude of the displacements is arbitrary. Blue, orange, green, red and purple curves correspond to modes $k = 2 - 6$, respectively.

of the displacements is arbitrary. We clarify that the radius from which each mode in each panel bifurcates is different, as their critical voltage is different, and hence the underlying configuration is different too.

## 6. Summary

We have investigated prismatic bifurcations of soft dielectric tubes subjected to radial voltage, using the theory of Dorfmann and Ogden (2010). Our first stage was to develop the equations that govern incremental deformations in a tube which was finitely strained by a combination of radial voltage and mechanical stretch. Our model accounts for the electroelastic coupling, heterogeneous deformed configuration and elastomeric stiffening. To determine the bifurcation criterion, we have postulated diffuse mode solutions to the resultant equations, and derived their existence condition. We have numerically evaluated the bifurcation criterion for a representative tube with different mechanical constraints and varying wall thickness. In each case, the critical voltage found to trigger diffuse mode instabilities according to our bifurcation condition was compared to the critical voltage found by the Hessian stability criterion. The comparison shows that a tube without mechanical constraints may experience prismatic bifurcations even when the Hessian stability criterion is satisfied. Our comparison also shows that a mechanically constrained tube can develop diffuse mode instability, while considered stable according to the Hessian criterion.

## References

An, L., Wang, F., Cheng, S., Lu, T., & Wang, T. (2015). Experimental investigation of the electromechanical phase transition in a dielectric elastomer tube. *Smart Materials and Structures, 24*(3), 035006.

Bertoldi, K., & Gei, M. (2011). Instabilities in multilayered soft dielectrics. *Journal of the Mechanics and Physics of Solids, 59*(1), 18–42.

Bortot, E., & Shmuel, G. (2017). Tuning sound with soft dielectrics. *Smart Materials and Structures, 26*, 045028. doi:10.1088/1361-665X/aa6387.

Carpi, F., & De Rossi, D. (2004). Dielectric elastomer cylindrical actuators: electromechanical modelling and experimental evaluation. *Materials Science and Engineering C, 24*(4), 555–562.

Carpi, F., De Rossi, D., Kornbluh, R., Pelrine, R., & Sommer-Larsen, P. (2008). *Dielectric elastomers as electromechanical transducers: Fundamentals, materials, devices, models and applications of an emerging electroactive polymer technology*. Elsevier Science.

Cohen, N. (2017). Stacked dielectric tubes with electromechanically controlled radii. *International Journal of Solids and Structures, 108*, 40–48. https://doi.org/10.1016/j.ijsolstr.2016.09.014.
De Tommasi, D., Puglisi, G., Saccomandi, G., & Zurlo, G. (2010). Pull-in and wrinkling instabilities of electroactive dielectric actuators. *Journal of Physics D, 43*(32), 325501. doi:10.1088/0022-3727/43/32/325501.
deBotton, G., Tevet-Deree, L., & Socolsky, E. (2007). Electroactive heterogeneous polymers: Analysis and applications to laminated composites. *Mechanics of Advanced Materials and Structures, 14*, 13–22.
Díaz-Calleja, R., Llovera-Segovia, P., & Quijano-López, A. (2017). Complex bifurcation maps in electroelastic elastomeric plates. *International Journal of Solids and Structures, 113*, 70–84. https://doi.org/10.1016/j.ijsolstr.2016.12.021.
Díaz-Calleja, R., Riande, E., & Sanchis, M. (2008). On electromechanical stability of dielectric elastomers. *Applied Physics Letters, 93*(10), 101902. doi:10.1063/1.2972124.
Dorfmann, A., & Ogden, R. (2005). Nonlinear electroelasticity. *Acta Mechanica, 174*, 167–183.
Dorfmann, A., & Ogden, R. (2010). Nonlinear electroelastostatics: Incremental equations and stability. *International Journal of Engineering Science, 48*(1), 1–14. https://doi.org/10.1016/j.ijengsci.2008.06.005.
Dorfmann, L., & Ogden, R. (2014). Instabilities of an electroelastic plate. *International Journal of Engineering Science, 77*, 79–101. doi:10.1016/j.ijengsci.2013.12.007.
Ertepinar, A. (1978). Stability and vibrations of thick-walled tubes subjected to finite twist and external pressure. *International Journal of Solids and Structures, 14*(9), 715–722. doi:10.1016/0020-7683(78)90030-6.
Gei, M., Colonnelli, S., & Springhetti, R. (2014). The role of electrostriction on the stability of dielectric elastomer actuators. *International Journal of Solids and Structures, 51*(3–4), 848–860. https://doi.org/10.1016/j.ijsolstr.2013.11.011.
Haughton, D., & Ogden, R. (1979a). Bifurcation of inflated circular cylinders of elastic material under axial loading–I. Membrane theory for thin-walled tubes. *Journal of the Mechanics and Physics of Solids, 27*, 179–212.
Haughton, D., & Ogden, R. (1979b). Bifurcation of inflated circular cylinders of elastic material under axial loading–II. Exact theory for thick-walled tubes. *Journal of the Mechanics and Physics of Solids, 27*, 489–512.
Jiang, L., Betts, A., Kennedy, D., & Jerrams, S. (2016). Eliminating electromechanical instability in dielectric elastomers by employing pre-stretch. *Journal of Physics D: Applied Physics, 49*(26), 265401.
Keplinger, C., Li, T., Baumgartner, R., Suo, Z., & Bauer, S. (2012). Harnessing snap-through instability in soft dielectrics to achieve giant voltage-triggered deformation. *Soft Matter, 8*, 285–288.
Kornbluh, R. (2008). Chapter 8- Fundamental configurations for dielectric elastomer actuators. In F. Carpi, D. De Rossi, R. Kornbluh, R. Pelrine, & P. Sommer-Larsen (Eds.), *Dielectric elastomers as electromechanical transducers* (pp. 79–90). Amsterdam: Elsevier. doi:10.1016/B978-0-08-047488-5.00008-3. http://www.sciencedirect.com/science/article/pii/B9780080474885000083
Leng, J., Liu, L., Liu, Y., Yu, K., & Sun, S. (2009). Electromechanical stability of dielectric elastomer. *Applied Physics Letters, 94*(21), 211901. doi:10.1063/1.3138153.
Li, B., Chen, H., Qiang, J., Hu, S., Zhu, Z., & Wang, Y. (2011). Effect of mechanical pre-stretch on the stabilization of dielectric elastomer actuation. *Journal of Physics D: Applied Physics, 44*(15), 155301.
Li, T., Keplinger, C., Baumgartner, R., Bauer, S., Yang, W., & Suo, Z. (2013). Giant voltage-induced deformation in dielectric elastomers near the verge of snap-through instability. *Journal of the Mechanics and Physics of Solids, 61*(2), 611–628.
Liu, L. (2013). On energy formulations of electrostatics for continuum media. *Journal of the Mechanics and Physics of Solids, 61*(4), 968–990. https://doi.org/10.1016/j.jmps.2012.12.007.
Lu, T., An, L., Li, J., Yuan, C., & Wang, T. (2015). Electro-mechanical coupling bifurcation and bulging propagation in a cylindrical dielectric elastomer tube. *Journal of the Mechanics and Physics of Solids, 85*, 160–175. doi:10.1016/j.jmps.2015.09.010.
Lu, T., Cheng, S., Li, T., Wang, T., & Suo, Z. (2016). Electromechanical catastrophe. *International Journal of Applied Mechanics, 08*(07), 1640005. doi:10.1142/S1758825116400056.
Melnikov, A., & Ogden, R. (2016). Finite deformations of an electroelastic circular cylindrical tube. *Zeitschrift für Angewandte Mathematik und Physik, 67*(6), 140. doi:10.1007/s00033-016-0733-0.
Ogden, R., Steigmann, D., & Haughton, D. (1997). The effect of elastic surface coating on the finite deformation and bifurcation of a pressurized circular annulus. *Journal of Elasticity, 47*, 121–145.
O'Halloran, A., O'Malley, F., & McHugh, P. (2008). A review on dielectric elastomer actuators, technology, applications, and challenges. *Journal of Applied Physics, 104*(7).
Pelrine, R., Kornbluh, R., & Joseph, J. (1998). Electrostriction of polymer dielectrics with compliant electrodes as a mean of actuation. *Sensors and Actuators A, 64*, 77–85.
Pelrine, R., Kornbluh, R., Joseph, J., Heydt, R., Pei, Q., & Chiba, S. (2000). High-field deformation of elastomeric dielectrics for actuators. *Material Science and Engineering, 11*, 89–100.
Pelrine, R., Kornbluh, R., Pei, Q., & Joseph, J. (2000). High-speed electrically actuated elastomers with strain greater than 100%. *Science, 287*, 836–839.
Plante, J., & Dubowsky, S. (2006). Large-scale failure modes of dielectric elastomer actuators. *International Journal of Solids and Structures, 43*(25–26), 7727–7751.
Shivapooja, P., Wang, Q., Orihuela, B., Rittschof, D., López, G., & Zhao, X. (2013). Bioinspired surfaces with dynamic topography for active control of biofouling. *Advanced Materials, 25*(10), 1430–1434. doi:10.1002/adma.201203374.
Shmuel, G. (2015). Manipulating torsional motions of soft dielectric tubes. *Journal of Applied Physics, 117*(17), 174902. https://doi.org/10.1063/1.4919668.
Shmuel, G., & deBotton, G. (2013). Axisymmetric wave propagation in finitely deformed dielectric elastomer tubes. *Proceedings of the Royal Society A, 469*(2155).
Siboni, M., Avazmohammadi, R., & Castañeda, P. (2014). Electromechanical instabilities in fiber-constrained, dielectric-elastomer composites subjected to all-around dead-loading. *Mathematics and Mechanics of Solids*. doi:10.1177/1081286514551501.
Singh, M., & Pipkin, A. (1966). Controllable states of elastic dielectrics. *Archive for Rational Mechanics and Analysis, 21*, 169–210.
Su, Y., Zhou, W., Chen, W., & Lü, C. (2016). On buckling of a soft incompressible electroactive hollow cylinder. *International Journal of Solids and Structures, 97–98*, 400–416. doi:10.1016/j.ijsolstr.2016.07.008.
Suo, Z., Zhao, X., & Greene, W. (2008). A nonlinear field theory of deformable dielectrics. *Journal of the Mechanics and Physics of Solids, 56*(2), 467–486.
Wang, Q., Tahir, M., Zhang, L., & Zhao, X. (2011). Electro-creasing instability in deformed polymers: experiment and theory. *Soft Matter, 7*, 6583–6589. doi:10.1039/C1SM05645J.
Wu, B., Su, Y., Chen, W., & Zhang, C. (2017). On guided circumferential waves in soft electroactive tubes under radially inhomogeneous biasing fields. *Journal of the Mechanics and Physics of Solids, 99*, 116–145. doi:10.1016/j.jmps.2016.11.004.
Yang, S., Zhao, X., & Sharma, P. (2017). Revisiting the instability and bifurcation behavior of soft dielectrics. *Journal of Applied Mechanics-Transaction of the ASME, 84*(3), 031008. doi:10.1115/1.4035499.
Zhao, X., & Suo, Z. (2007). Method to analyze electromechanical stability of dielectric elastomers. *Applied Physics Letters, 91*, 061921.
Zhao, X., & Suo, Z. (2010). Theory of dielectric elastomers capable of giant deformation of actuation. *Physical Review Letters, 104*(17), 178302. doi:10.1103/PhysRevLett.104.178302.
Zhao, X., & Wang, Q. (2014). Harnessing large deformation and instabilities of soft dielectrics: Theory, experiment, and application. *Applied Physics Review, 1*(2), 021304. doi:10.1063/1.4871696.
Zhou, J., Hong, W., Zhao, X., Zhang, Z., & Suo, Z. (2008). Propagation of instability in dielectric elastomers. *International Journal of Solids and Structures, 45*(13), 3739–3750. doi:10.1016/j.ijsolstr.2007.09.031. Special Issue Honoring K.C. HwangFracture, Plasticity, Micro- and NanomechanicsSpecial Issue Honoring K.C. Hwang

Zhou, J., Jiang, L., & Khayat, R. (2014). Electromechanical response and failure modes of a dielectric elastomer tube actuator with boundary constraints. *Smart Materials and Structures, 23*(4), 045028. doi:10.1088/0964-1726/23/4/045028.

Zhu, J., Stoyanov, H., Kofod, G., & Suo, Z. (2010). Large deformation and electromechanical instability of a dielectric elastomer tube actuator. *Journal of Applied Physics, 108*(7), 074113.

Zurlo, G., Destrade, M., De Tommasi, D., & Puglisi, G. (2017). Catastrophic thinning of dielectric elastomers. *Physical Review Letters, 118*, 078001. doi:10.1103/PhysRevLett.118.078001.